Hydrogen transport in superionic system $Rb_3H(SeO_4)_2$: A revised cooperative migration mechanism

N. Pavlenko,[1] A. Pietraszko,[2] A. Pawlowski,[3] M. Polomska,[3] I. V. Stasyuk,[1] and B. Hilczer[3]
[1]*Institute for Consensed Matter Physics, 79011 Lviv, Ukraine*
[2]*Institute of Low Temperatures and Structural Research PAN, PL-50-950 Wroclaw 2, Poland*
[3]*Institute of Molecular Physics PAN, Smoluchowskiego 17, PL-70169 Poznan, Poland*
(Received 4 March 2011; revised manuscript received 15 July 2011; published 19 August 2011)

We performed density functional studies of electronic properties and mechanisms of hydrogen transport in $Rb_3H(SeO_4)_2$ crystal that represents technologically promising class $M_3H(XO_4)_2$ of proton conductors (M = Rb, Cs, NH_4; X = S,Se). The electronic structure calculations show a decisive role of lattice dynamics in the process of proton migration. In the obtained revised mechanism of proton transport, the strong displacements of the vertex oxygens play a key role in establishing the continuous hydrogen transport and in achieving low activation energies of proton conduction that is in contrast to the standard two-stage Grotthuss mechanism of proton transport. Consequently, any realistic model description of proton transport should inevitably involve the interactions with the sublattice of the XO_4 groups.

DOI: 10.1103/PhysRevB.84.064303 PACS number(s): 71.15.Mb, 71.20.−b, 66.30.Dn

I. INTRODUCTION

In the past few years there has been a continuous increase of research activity in the field of hydrogen conductors. This can be explained by great technological advances in the use of hydrogen conducting materials for applications in solid-state hydrogen fuel cells, hydrogen storage, and electrochemical devices.[1–4] A central problem in fuel-cell and hydrogen batteries technology is the development of cheap and efficient materials for electrochemical elements that can be used for the chemical storage and transformation of chemical to electrical energy. In the functional properties of hydrogen devices, the transport of hydrogen through the conducting part to cathode plays a key role that makes the proton transport mechanisms one of the central problems of current experimental and theoretical studies.[5–7]

In the wide range of proton conducting materials, the crystals with superionic phases $M_3H(XO_4)_2$ (M = Rb,Cs, NH_4; X = S,Se) are of special interest due to their high proton conductivity coefficients that in the high-temperature disordered state can reach values of the order 10^{-2}–10^{-1} Ω^{-1} cm^{-1}. In these phases, the quasi-two-dimensional proton transport is characterized by a dynamically disordered network of virtual hydrogen bonds dynamically establishing between the vertex oxygens O(2) of nearest groups XO_4. Although on the first sight the transport of protons in hexagonal (001) planes seems to be quite a straitforward process explained in terms of the two-stage Grotthuss mechanism,[8–10] the real mechanism of proton migration is still not sufficiently well examined and understood. The reason for this difficulty is a complex cooperative character of proton migration that should strongly interact with the dynamics of the ionic environment, a fact supported by numerous experimental Raman, infrared, x-ray, and NMR spectroscopy studies.[11–17]

In the theoretical works,[16,18–22] the two-stage Grotthuss mechanism is frequently considered within phenomenological free-particle approches that typically contain two stages: (i) translation of proton within a hydrogen bond between the nearest ionic groups XO_4 and (ii) interbond proton transfer related to reorientations of the ionic groups XO_4. However, the experimental studies demonstrate that the transport of protons is a highly complex process that can be characterized as a transfer of hydrogen ion in the course of the reactions of creation and breaking of HXO_4 bonds. As a consequence of such reacting environment with dynamically redistributing electronic density, the protons in conducting materials cannot be described as almost free particles.

Despite the existing theoretical studies of the low-temperature proton ordered phases and proton conduction in $M_3H(XO_4)_2$ by phenomenological models,[18–22] to date there have been no first-principles investigations of these systems. The recent first-principles molecular dynamics studies of superprotonic phase transition in a related superionic system $CsHSO_4$[23] were focused on the structural transformations and reorientational motion of HSO_4^- groups, without the studies of the proton migration mechanism. Another *ab initio* study of the proton conduction in $CsHSO_4$ has been devoted to the estimation of diffusion barriers, without a detailed consideration of the role of oxygen network in the proton transport mechanism.[24] The lack of the first-principles investigations of the transport mechanism in $M_3H(XO_4)_2$ can be explained by highly complicated crystal structure of these systems involving several structural transformations that makes *ab initio* calculations extremely time-consuming and challenging. Our present studies of the hydrogen transport are based on the density functional theory (DFT) with the use of the linearized augmented plane-wave method (LAPW) implemented in the WIEN2k package.[25] The local density approximations (LDA) with nonlinear core corrections and generalized gradient approximations (GGA) of the DFT developed by Perdew, Burke, and Ernzerhof[26] and Perdew and Zunger[27] have been employed in our calculations. In the GGA, the additional gradient terms of the electron density are added to the exchange-correlation energy and its corresponding potential, which is beyond the LDA of the DFT. In our studies of the proton migration paths, we also employ a nudged-elastic-band method within the pseudopotential approach implemented in the QUANTUM ESPRESSO package[28] which allows to perform the dynamical relaxation of the atomic surrounding along the steps of the proton conduction processes.

As an attempt to account for the coupling of mobile protons with the dynamical distortions of the groups XO_4, the existing microscopic description of the proton transport considers the interaction of protons with the displacements of the vertex oxygens O(2) of XO_4 involved in the hydrogen bonding.[21] Such a coupling is presented in terms of the interaction of proton charge with the optical phonon modes corresponding to the antiphase stretching vibrations of the O(2) ions and is classified in terms of "protonic polaron" concept. The calculated in this approach coefficients of the proton conductivity are consistent with the experimental measurements performed in the superionic phases.[29] However, the polaronic concept introduced in Ref. 21 involves a number of phenomenological parameters, like polaron binding energy, which have been estimated by the fitting of the calculated conductivity to the experimentally measured values. To verify the role of the dynamical distortions in the proton migration mechanism, in this work we present a detailed DFT study of the mechanism of hydrogen migration in the system $Rb_3H(SeO_4)_2$, which belongs to the $M_3H(XO_4)_2$ class.

To investigate the role of the proton environment, two aspects of the hydrogen transport have been analyzed. The first aspect is related to the structure and positioning of hydrogen-bonded oxygen ions O(2) in the dynamical network. The present DFT calculations demonstrate the strong displacements of O(2) from the high-symmetry positions on the threefold axis in the equilibrium state, which allows us to verify the concepts of the O(2) structural positioning discussed in the previous x-ray and NMR studies.[15,30] As the second aspect, we have analyzed the migration paths of protons in the configuration of instantaneously relaxed atoms. The performed DFT calculations allow us to derive the energy profiles along the proton migration paths and to investigate the displacements of each atom involved in the proton surrounding. As a result, the present studies make it possibile to obtain the first-principles estimates of the hydrogen bond lengths and energetic parameters involved in the phenomenological modeling and to verify the concept of protonic polarons introduced in the previous phenomenological description of proton transport. Our findings also allow us to improve several experimental conclusions obtained in the previous x-ray and NMR experiments with $Rb_3H(SeO_4)_2$,[15,30] in particular, to clarify the positioning of the vertex oxygens O(2) during the proton migration and to examine the proton positions on the hydrogen bond at the intrabond proton transfer. As a result, the present DFT results demonstrate a central role of oxygen displacements for the migration of hydrogen and emphasize in this way a key role of the proton environment in establishing the proton transport.

The rest of the paper is organized in three sections. In Sec. II, the theoretical methods employed in our studies are discussed. Section III presents the results of the electronic structure calculations and of the calculations of the proton migration paths and oxygen positioning. In Sec. IV, we summarize the main results and conclusions of our work.

II. THEORETICAL MODELS AND METHODS

A. Structural concepts of the hydrogen-bonded network

In the high-temperature disordered phase of $Rb_3H(SeO_4)_2$ schematically shown in Fig. 1(a), hydrogen transport occurs

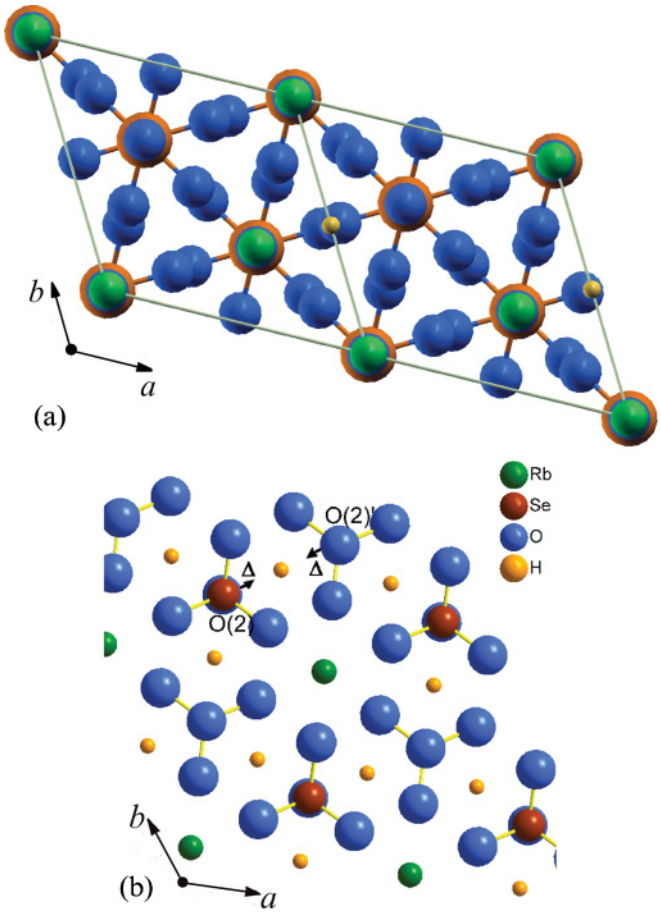

FIG. 1. (Color online) (a) Schematical presentation of the crystal structure of $Rb_3H(SeO_4)_2$ in the superionic phase in projection on the hexagonal (001) plane, where the rhombohedral unit cell of $R\bar{3}m$ symmetry is doubled along the (100) direction. One of the virtual hydrogen bonds with the proton centered on the bond is shown for simplicity. The small orange circles denote the protons, and the oxygen atoms are indicated by blue, Rb atoms by green, and Se by brown circles. (b) Atomic configuration of hydrogen-bonded network of SeO_4 tetrahedra in superionic phase in the proton conducting layer corresponding to a slab ($-0.13c \leqslant z \leqslant 0.13c$) in the hexagonal (x,y) plane, with the lattice constant $c = 22.629$ Å. The orange circles indicate the possible positions for the disordered protons occupied with a probabibity 1/3.

in a network of "virtual" (equally probable) hydrogen bonds that are occupied by a proton with equal probability 1/3. This network [see Fig. 1(b) for details] is established between the vertex oxygens O(2) of the tetrahedra SeO_4 that can be chemically bonded to the three nearest tetrahedra by hydrogen bonds.

The experimentally deduced structure of the network of hydrogen-bonded tetrahedra at $T = 456$ K projected on the (001) plane is represented by the electronic difference density map in Fig. 2. This map has been calculated from the x-ray diffraction data using SHELXL-93 programs. The central feature detected in Fig. 2 is a disorder of the hydrogen-bonded vertex oxygens O(2) (shown by red dots) between three structurally equivalent positions. The hydrogen bonds are schematically presented by the solid lines where the double black dots denote the positions for proton in a double-well potential.

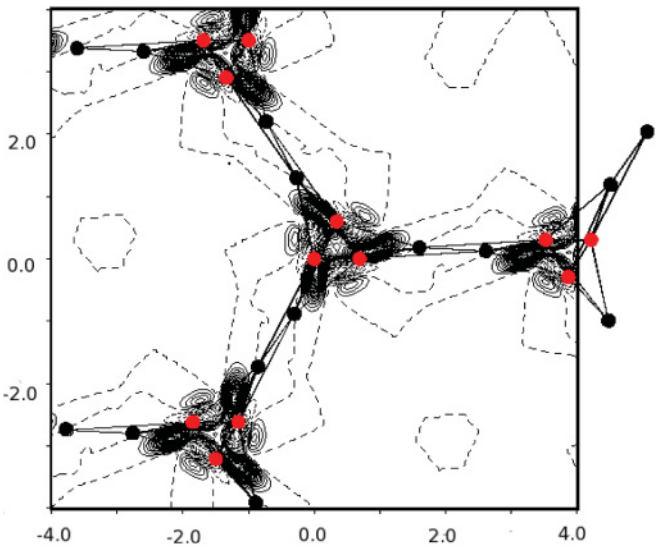

FIG. 2. (Color online) Electron charge density maps of the nearest neighboring SeO_4 groups of $Rb_3H(SeO_4)_2$ in the disordered superionic state at $T = 456$ K. Here the red dots show the possible positions of the vertex oxygens O(2) around the threefold axis and the black dots correspond to the location of disordered protons on O(2)-H-O(2)′ hydrogen bonds.

In the earlier work by Baranov *et al.*,[15] a different concept of the structure of hydrogen-bonded network is proposed for the analysis of the x-ray diffraction data. In this concept, the oxygens O(2) are statically located in high-symmetry positions on threefold axis. which also implies a static character of the of SeO_4 tetrahedra and leads to a possibility of the movement of free protons in the disordered superionic phase. Therefore, the arrangement of the vertex oxygens O(2) is still an open question that has prime importance for the understanding the nature of proton transfer mechanism in these systems.

In the first concept of the structural arrangement of O(2) in the superionic phase of $Rb_3H(SeO_4)_2$ signified in Ref. 15, the oxygens O(2) are located in the high-symmetry positions on the threefold axis and form weak hydrogen bonds with the length of the covalent bond O(2)-H approaching 1.76 Å. In distinction from the high-symmetry case, the second type of oxygen arrangement discussed in Ref. 15 and 17 assumes the distortions of O(2) from the threefold axis toward the hydrogen at the formation of the O(2)-H-O(2)′ bond. To prevent a break of high symmetry in the disordered superionic phase caused by such distortions, a dynamical disorder of each O(2) between three equally probable positions is assumed. These positions are related to each other by a rotation by 120° around the threefold axis [see Fig. 2 where the three equivalent positions of distorted O(2) are marked by red dots].

To analyze the equilibrium positions of the oxygens O(2), we performed the GGA calculations of the total energy of the system for the different values of the displacements Δ of the oxygen O(2) from the positions of the threefold axis toward a migrating proton, a process which is schematically shown in Fig. 1(b). In the calculations of the electronic structure of $Rb_3H(SeO_4)_2$, the lattice constants of the unit cell of the trigonal $R\bar{3}m$ symmetry in hexagonal coordinates were fixed to the values obtained from the structural analysis[15]: $a = 6.118$ Å and $c = 22.629$ Å. Technical details include a GGA method developed by Perdew, Burke, and Ernzerhof[26] on a $4 \times 2 \times 3$ $\boldsymbol{k}$-point grid representing a mesh of 40 $\boldsymbol{k}$-points in the first Brillouin zone. The comparison of the total energy calculated for the mesh of 80 $\boldsymbol{k}$-points gives the difference between the total energies $E_{\text{tot}}(80) - E_{\text{tot}}(40) = 0.00136$ eV that allows us to use the 40 $\boldsymbol{k}$-point mesh for the GGA calculations.

The full-potential method[25] employs an expansion of the electronic potential inside the atomic spheres via a full number of the electronically occupied local orbitals (Rb, Se, O, and H atoms in our case), whereas the potential outside the spheres is constructed as a plane-wave expansion with a plane-wave cutoff given by 667 eV. Such a method allows to achieve high accuracy in the description of the electronic structure, total energy, and electronic density of states. The dynamical disorder in the superionic state cannot be directly described in the static density functional calculations. As a consequence, in a generated model unit cell, only a single hydrogen bond is selected from the three virtual hydrogen bonds near each SeO_4 group that leads to a lowering of the symmetry of the system from the rhombohedral to monoclinic. In this case, the generated structure can be considered as a static snapshot of the dynamically disordered superionic state. In the studies of the hydrogen transport mechanism we also considered a doubled unit cell, where the initial orientations of the two hydrogen bonds in the cell are chosen randomly, each bond can be dynamically broken and created in a chain of intermediate configurations generated by the nudged elastic band (NEB) method.[28,31]

In the studies of the transport mechanism, each atomic configuration has been structurally relaxed. The relaxation involves the optimization of the atomic positions by the minimization of the total energy and forces acting on the atoms in the generated unit cell. For the structural optimization, we use a Newton scheme described in Ref. 31. A comparison of different relaxed static configurations allows us to calculate the energy barriers for the proton migration. With the obtained zero-temperature results, we also analyze the influence of temperature on the activation energies of the proton transport.

B. Modeling the hydrogen migration paths

To analyze in detail the paths for the hydrogen migration in the relaxed surrounding, we employed the nudged-elastic-band (NEB) method implemented in the QUANTUM-ESPRESSO (QE) package of the DFT calculations with the use of plane-wave basis sets and pseudopotentials.[28,31] In these calculations, for the atomic cores of Rb, H, Se, and O, we employ the Perdew-Zunger (PZ) norm-conserving pseudopotentials with nonlinear core corrections.[27] Our choice of pseudopotentials is justified by the fact that all characteristic features of the electronic structure calculated with the use of the full potential WIEN2k GGA code [Fig. 3(a)] and obtained with the PZ pseudopotentials [Fig. 3(b)] are consistent in the energy window ($E_F - 7.0$ eV; $E_F + 1$ eV), where E_F is the Fermi energy. Specifically, both approaches allow us to describe the characteristic DOS peaks related to the O(2)-2p orbitals (the energy range between E_F and $E_F - 5$ eV in Fig. 3) and the DOS peak related to the 1s orbital of H at the energy

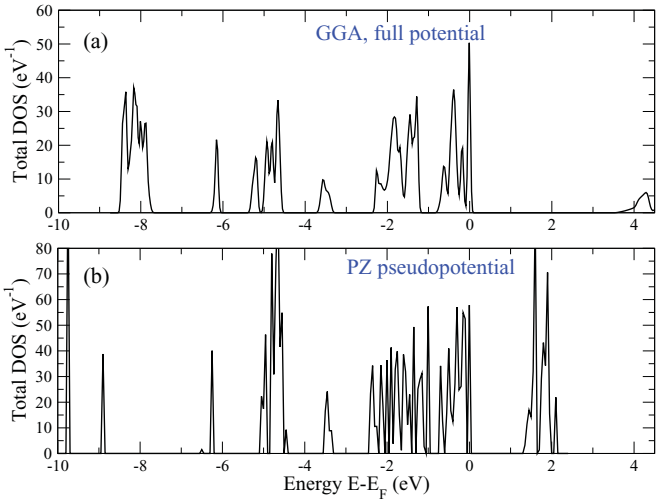

FIG. 3. (Color online) Total density of states calculated (a) in the GGA (Perdew, Burke, and Ernzerhof; Ref. 26) using the full potential approach of Ref. 25 and (b) in the LDA using norm-conserving atomic pseudopotential approach with nonlinear core corrections implemented by Perdew and Zunger; see Ref. 27. The zero energies correspond to the Fermi levels.

value about −6.1 eV [Fig. 3(a)] that corresponds to the peak at about −6.2 eV in Fig. 3(b). In the GGA approach, the energy gap between the highest filled and lowest empty electronic states is about 3.5 eV [Fig. 3(a)] that is close to experimentally discussed gap about 4 eV[32] in related compounds. The GGA gap is larger then the gap about 1.3 eV obtained by the LDA method [Fig. 3(b)] due to the usual underestimation of the gap in the LDA calculations, which does not influence the results of the NEB studies based on the calculations of the total energy. Also, we would like to note that a detailed comparison of the electronic and optical properties of several compounds like Rb_2O and Li_2O related to the constituents of $Rb_3H(SeO_4)_2$ calculated in the LDA and GGA approaches shows a good consistency with the available experimental results.[33] As the low-temperature electronic properties calculated by these two approaches are consistent, we conclude that the PZ pseudopotential approach implemented in the QE code is sufficient to capture the physical features of the hydrogen migration in our system.

In contrast to the almost free motion of the hydrogen implemented in a wide range of the models of hydrogen transport, in the present work we consider the migration of hydrogen as a *cooperative process*, the feature that can be described by the NEB approach.[28,31] Specifically, for each stage of the hydrogen transport, this process involves a relaxation of the atomic positions and of the distances between the different atoms. In our analysis, to better relax the positions of the atoms neighboring to H, we perform a doubling of the unit cell that now includes four SeO_4 groups and two protons [see Fig. 8(a) for details]. For each position of the hydrogen in the unit cell, the coordinates of all neighboring atoms were relaxed until the forces acting on the atoms reached their minima. In these calculations, we use the plane-wave cutoff 1020 eV and the energy cutoff for charge and potential given by 2040 eV.

In the NEB approach, the relaxation of the atomic positions along the hydrogen migration path is performed by the minimization of the total energy of each intermediate configuration (image). These images correspond to different positions of H on the migration path and produced by the optimization of a specially generated object functional (action) with the consequent minimization of the spring forces perpendicular to the path. In our calculations, the convergence criteria for the norm of the force orthogonal to the path is achieved at the values below 0.05 eV/Å.

III. RESULTS AND DISCUSSION

A. Vertex oxygens O(2)

The experiments (see Ref. 29) show that in $M_3H(XO_4)_3$ crystals the temperature of the superionic phase transition T_S does not depend on the deuterization. Moreover, the neutron diffraction results[30] do not distinguish two distinct hydrogen positions on the bonds and justify a representation of the hydrogen atom in flat single-minimum potentials. Consequently, in the present studies of the positioning of O(2), the initial proton positions are fixed to the centers of hydrogen bonds. In Fig. 1, such a single-well approximation is identified by the centering of proton between the oxygens O(2).

To study the modification of the total energy caused by the relaxation of the vertex oxygens, the positions of O(2) on a selected hydrogen bond were shifted by a distance Δ, while the coordinates of other atoms were kept in the undistorted high-symmetry state. Figure 4 demonstrates the variation of the total energy of the system $E(\Delta) - E(\Delta = 0)$ with the increase of the O(2) displacement parameter Δ. One can see that the lowest value of $E(\Delta)$ corresponds to $\Delta = 0.5$ Å that implies a stabilization of a short hydrogen bond O(2)-H-O(2)′ of a length 2.54 Å where the length of the covalent bond O(2)-H equals 1.27 Å. It is remarkable that, despite the central-point approximation for the proton within the hydrogen bonds, the obtained length of the H-bond is typical for double-well H bonds and is consistent with the

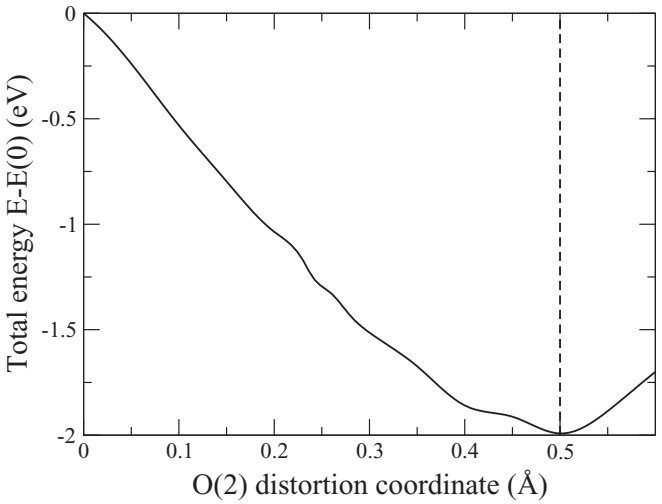

FIG. 4. Total system energy as a function of the O(2) distortion parameter Δ. Here Δ is the displacement of O(2) with respect to its high-symmetry position on the threefold axis.

TABLE I. Hydrogen bond length parameters (in Å) in the superionic phase of $Rb_3H(SeO_4)_2$ determined from the experiments and calculated by the O(2) relaxation in the full-potential GGA.

GGA [O(2) relaxation]	Ref. 15	Ref. 30	Ref. 11
2.54	2.51	2.594	2.58

results of x-ray and neutron scattering studies,[15,17,30] which becomes clear from the comparison of different data with the present results presented in Table I. Consequently, our findings clearly support the second concept of the oxygen-distorted network structure that is characterized by the two types of dynamical disorder in the superionic phase: (i) the statistical disorder of the hydrogens between the virtual hydrogen bonds in hexagonal planes and (ii) the disorder of the vertex oxygens between three symmetry-related positions around the threefold axis indicated in Fig. 1(b).

To demonstrate the influence of the displacements of O(2) on the electronic properties, we have analyzed the projected atomic densities of electronic states for $\Delta = 0$ and $\Delta = 0.5$ Å that are presented in Fig. 5. The considered two types of the structural positioning of O(2) can be characterized by a substantial electronic hybridization of H 1*s* orbitals and 2*p* orbitals of O(2). In Fig. 5, the *s*-*p* hybridization can be identified by the density peaks at the energies about −3.5 eV and in the range (−5.5)–(−6) eV below the Fermi energy (for $\Delta = 0.5$ Å, these peaks are marked by a dashed line). The DOS peaks at about −18 eV imply also a strong hybridization between H 1*s* and O(2) 2*s* orbitals. The displacements of O(2) from the high-symmetry positions lead to a shortening of the O(2)-H distances and consequently to a significant increase of the *s*-*p* hybridization peaks at −6 eV. Moreover, the O(2) distortions result in the emergence of new strongly hybridized state at −9.5 eV. In addition, the displacements of O(2) induce the distortions of the SeO_4 tetrahedra that results

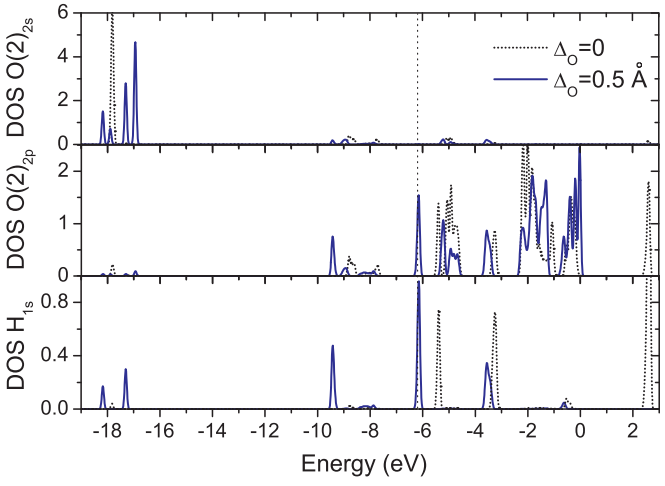

FIG. 5. (Color online) Projected density of states of the oxygens O(2) and hydrogens calculated by the GGA method. The cases $\Delta = 0$ and $\Delta = 0.5$ Å correspond to the hydrogen bonds between SeO_4 groups (a) with high-symmetry positions of O(2) on the threefold axis and (b) with the displacements of O(2) from the threefold positions toward the proton. The zero energy corresponds to the Fermi level.

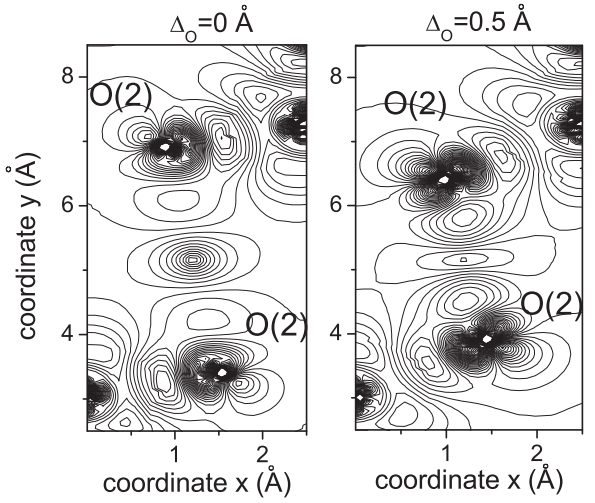

FIG. 6. Electronic difference density contours (crystalline renormalized by the superimposed atomic densities) for the hydrogen bonds O(2)-H-O(2). Here the oxygens O(2) are located on the threefold axis (left panel) and displaced from this axis toward the hydrogen on the bond (right panel).

in the lowering of the local symmetry and in the split of high hybridized peaks around −18 eV (Fig. 5, case $\Delta = 0.5$ Å). In the considered model unit cell, instead of the virtual H bonds we consider a number of selected configurations with the fixed H bonds near each SeO_4 group. In a real statistically disordered system one may expect that the obtained split of the hybridization peaks will be smoothed by the dynamical disorder.

The redistribution of the electronic charge density due to the distortions of O(2) causes the accumulation of the electron charge on the obtained short hydrogen bonds, the effect observed in the contours of the difference charge density in Fig. 6. Consequently, in the superionionic phase, the formation of the strong virtual hydrogen bonds should be also identified by a remarkable increase of the electron density between the O(2) ions, which is consistent with the experimentally obtained electron density map of Fig. 1.

B. Rotational stage in the full potential calculations

Based on the results obtained for the positions of the hydrogen-bonded O(2), it is possible to study the mechanisms and paths of the hydrogen migration. In our analysis, the special focus is put on the rotational stage of the Grotthuss transport mechanism. In its classical description, this stage involves the rotational motion of the $HSeO_4$ group around the threefold axis determined by a rotation angle α [see Fig. 7(b) where the rotation stage is schematically shown] and the consequent formation of a new hydrogen bond between the rotated group and the nearest SeO_4 tetrahedron approached by this rotation.

First, we analyze a possibility of the rotational step as an independent stage of the proton transport mechanism. In this case, the hydrogen with the covalently bonded oxygen O(2) is allowed to rotate around the nearest SeO_3 group while the positions of all the surrounding atomic groups are fixed. In such a rotational stage, we have calculated the variation of

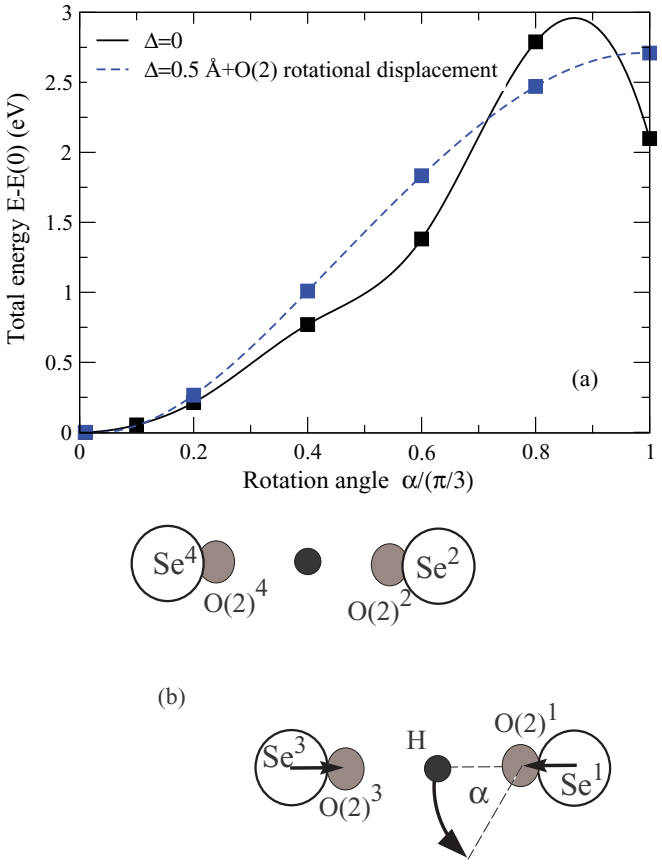

FIG. 7. (Color online) (a) Energy profiles for the rotation of hydrogen around the group $(SeO_4)^1$. The case $\Delta = 0$ corresponds to the oxygen $O(2)^1$ located on the threefold axis and fixed during the rotation of H. For $\Delta = 0.5$ Å, $O(2)^1$ is displaced by a distance Δ and rotates jointly with the hydrogen. (b) Shematical view of the rotation stage of the transport mechanism. The short arrows indicate the displacements of the oxygens O(2) from the threefold positions toward the proton, the large circles denote SeO_3 groups, and α is the rotation angle of O(2)-H covalent bond.

the total energy of the system due to the rotations. Similarly to the studies of the O(2) network in the previous section, we consider here two possible structural concepts for the rotational motion. In the first high-symmetry case, the oxygen $O(2)^1$ of the $H(SeO_4)^1$ group is fixed on the threefold axis ($\Delta = 0$), whereas in the second configuration the oxygen $O(2)^1$ is relaxed (displaced) by a distance $\Delta = 0.5$ Å from the threefold axis and rotates jointly with the hydrogen by the angle α [the rotation of $O(2)^1$-H covalent bond]. The resulting dependencies of the total energy on α are presented in Fig. 7.

It is remarkable that both high-symmetry and $O(2)^1$-H-rotated configurations are characterized by high-energy barriers (about 2.6–3 eV) between the initial position of proton and the transition state (TS) [Fig. 7(a)] that corresponds to the intermediate value of the rotation angle α about $\pi/3$. The high energy barriers *absolutely exclude any independent motion of proton in the conducting system*, a concept that is widely applied for the free electrons in metals. We also note the obtained values for the energy barriers are of the same order as the rotational barrier, 1.54 eV, calculated in Ref. 24 for the system $CsHSeO_4$ that prompts on the common physical aspects of the transport mechanisms in these classes of proton conductors.

Despite the high energy of the TS state, the dashed energy profile in Fig. 7 demonstrates a possibility for a partial rotation of the covalent bond $O(2)^1$-H by $\alpha = 20°$–$25°$, which has considerably lower barriers of about 0.3–0.7 eV. In the superionic state, such a partial rotation can be also accompanied by the displacements of the oxygen $O(2)^2$ of a neighboring group $(SeO_4)^2$ toward the hydrogen which would lower the energy barrier and could result in the formation of the new hydrogen bond $O(2)^1$-H-$O(2)^2$ with the consequent proton transfer to the group $(SeO_4)^2$. As a conclusion, the rotational motion of protons should also involve the relaxation of the oxygens O(2) of more distant SeO_4 groups.

C. Hydrogen migration as a cooperative process

In the studies of hydrogen migration in a fully relaxed surrounding, we employ the NEB method discussed in Sec. II B. Figure 8 shows the snapshots of the migration of the hydrogen H1 between the complexes $(SeO_4)^1$-$(SeO_4)^2$ and $(SeO_4)^2$-$(SeO_4)^3$ calculated by the NEB method. The obtained proton migration path can be described via several steps as outlined.

(i) The $O(2)^1$-H1 covalent bond is rotated around SeO_3^1-group that corresponds to the variation of the rotation angle α from its initial value $\pi/3$ to the value $\alpha = 0$ [Fig. 8(a), the path is schematically shown in Fig. 9(c)]. We note that this rotation fully corresponds to the rotational motion of H studied in the previous Sec. III B within the full potential approach, whereas the rotation in Sec. III B is performed in the opposite direction shown in Fig. 7(b) with the angle α changing from 0 to $\pi/3$. The comparison of the corresponding energy profiles calculated by use of the NEB method [Fig. 9(a), H1 coordinate r in the range $0 \leqslant r \leqslant 0.8$ Å] and in the full-potential approach (Fig. 7) shows that, despite the similar parabolic form, the energy barrier in the QE case $\Delta E(QE) = E(0) - E(r = 0.8)$ is about 1.0 eV which is much lower than the full-potential GGA value obtained from the difference $\Delta E(FP) = E(\alpha = \pi/3) - E(\alpha = 0) = 2.72$ eV. This comparison clearly demonstrates the key role of the structural relaxation in the NEB approach for the lowering the energy barriers for the proton transport.

In the further rotation of $O(2)^1$-H1 the H1 coordinate r changes from $r = 0.8$ to $r = 2$ Å that leads to a small increase of the total energy by about 0.2 eV in Fig. 9(a). In Fig. 9(a), the minimum of the total energy at $r = 0.8$ Å corresponds to the nearly zigzag alignment of the O(2)-H dimers [configuration presented in Fig. 8(b)], similarly to the low-temperature ordered phase III stabilized below the superionic transition temperature, see Refs. 15,20, and 34 for the detailed description of the structure of this phase. The rotation part in the range $0.8 \leqslant r \leqslant 2$ Å corresponds to the rotation stage of the Grotthuss transport mechanism.

In Fig. 9(a), the energy barrier for the hydrogen rotation step approaches 0.2 eV. Here the rotation barrier is estimated from the energy dependence between $r = 0.8$ [proton position indicated by the dashed line in Fig. 9(c)] and $r = 2$ Å.

(ii) The hydrogen is transferred from the oxygen ion $O(2)^1$ [in Fig. 8(b)] to the oxygen $O(2)^2$ [Fig. 8(c)]. Figure 10 presents

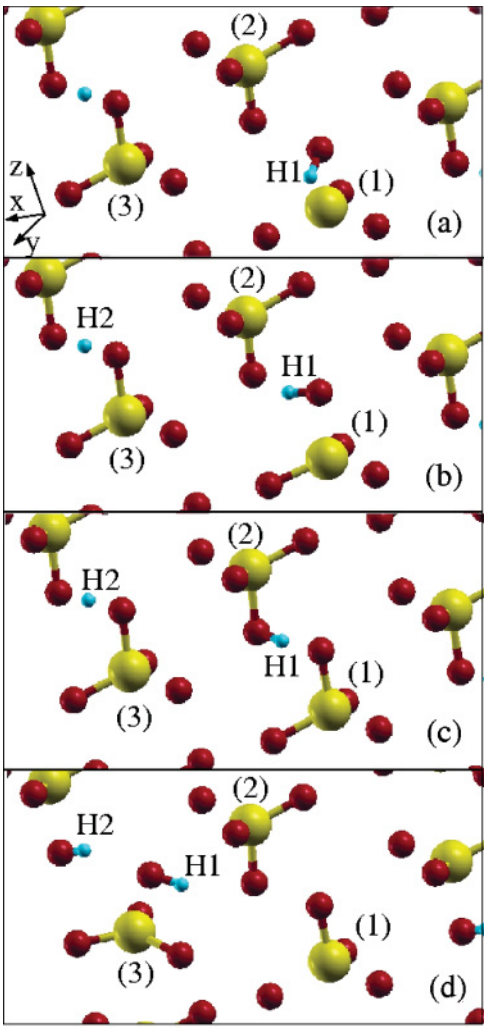

FIG. 8. (Color online) Snapshots demonstrating hydrogen migration between the neighboring groups $(SeO_4)^1$ and $(SeO_4)^3$. Here the Se, O and H atoms are represented by the yellow, red, and blue circles. Sections (a) and (b) show configurations with rotated $(SeO_4)^1$; that shown is (c) resulted from the transfer from (1) to (2) and rotation around $(SeO_4)^2$; and configuration (d) is obtained after the transfer of hydrogen between two tetrahedra $(SeO_4)^2$ and $(SeO_4)^3$.

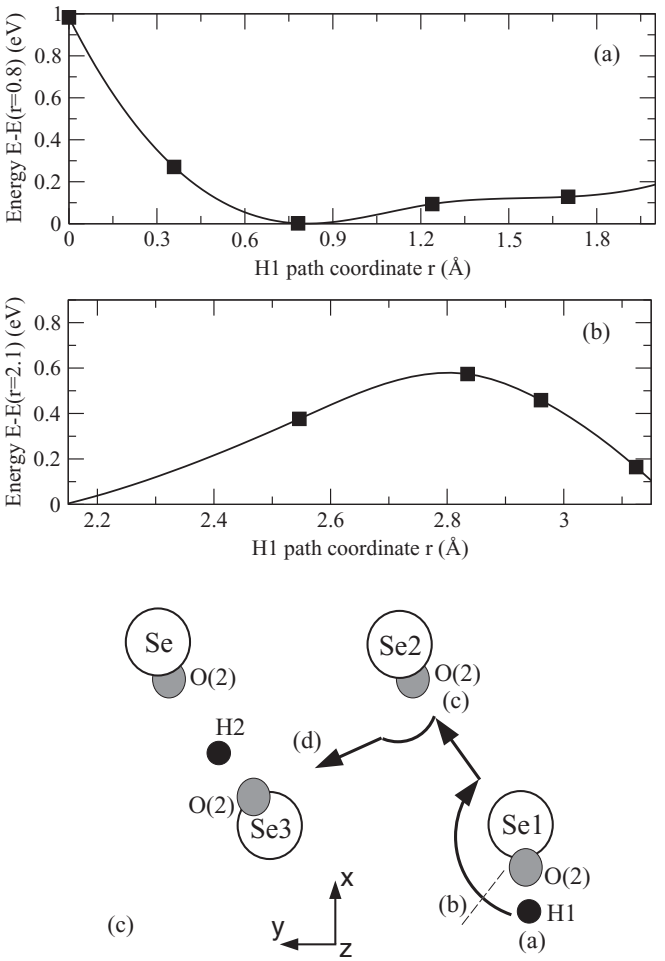

FIG. 9. Energy profiles for a migration of hydrogen between the tetrahedra $(SeO_4)^1$ and $(SeO_4)^2$. Here panel (a) corresponds to the rotation of the covalent bond H1-O(2) around the group $(SeO_4)^1$ and panel (b) corresponds to the transfer of H1 to the group $(SeO_4)^2$. (c) Schematic view of the migration path of H1 in the projection on the hexagonal (001) plane where the small symbols (a)–(d) correspond to the images in Fig. 8.

the displacements of the oxygens O(2) and the changes of the O(2)-O(2) distances during the migration of the hydrogen derived from the DFT(NEB) calculations. The proton transfer stage occurs in the range $(2 < r < 3)$ of the proton coordinate. It is remarkable that this range of r is characterized by significant displacements of $O(2)^1$ and $O(2)^2$, by 0.2–0.25 Å toward the hydrogen, and by the corresponding strong decrease of the distance between $O(2)^1$ and $O(2)^2$ from its inital value about 3 Å to the value 2.51 Å, which is very close to the results of the full-potential GGA studies (see Table I). In Fig. 10, the occurrence of the transfer of the hydrogen between $O(2)^1$ and $O(2)^2$ is identified by the minimal O(2)-O(2) distance and maximal displacement of $O(2)^1$ which is indicated by the red arrows in the plots. Table II presents the maximal (d_{OO}^{max}) and minimal (d_{OO}^{min}) lengths of the hydrogen bond during the transfer step calculated in the NEB approach that are compared to the corresponding experimentally obtained values. Despite the good agreement with the experimental maximal bond length, the calculated value of $d_{OO}^{min} = 2.51$ Å is in coincidence with the estimates of Ref. 15 for the superionic $Rb_3H(SeO_4)_2$ but is larger than the value 2.41 Å discussed in Ref. 17 for the similar system $(NH_4)_3H(SeO_4)_2$. The difference is possibly related to the influence of the dynamics of NH_4^+ groups in the superionic state that leads to additional softening of the structure and to the consequent increase of the O(2) displacements.[17]

(c) The $O(2)^2$-H1 covalent bond rotates and the hydrogen H1 moves toward the group $(SeO_4)^3$. The process of the $O(2)^2$-H1 rotation in the group $(SeO_4)^2$ is accompanied by the elongation of the covalent bond between the oxygen $O(2)^3$ and another proton H2 [shown in the left corner of part (c)] and by a strong displacement of the oxygen $O(2)^3$ toward the hydrogen H1 [Fig. 8(d)]. The displacement of the oxygen $O(2)^3$ leads to a decrease of the distance between $O(2)^2$ and $O(2)^3$ from its initial value 4.2 Å to the value 3.22 Å [Fig. 10(b)] and is essential for successful hydrogen migration to the group

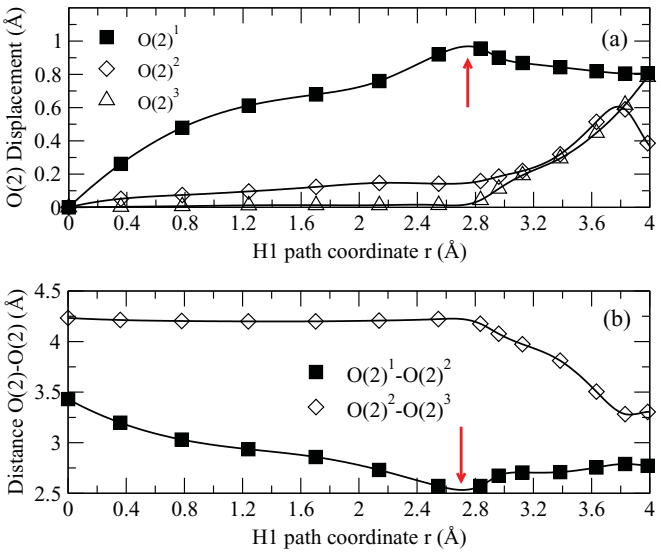

FIG. 10. (Color online) (a) Displacements of the vertex oxygens O(2) and (b) the change of the distance between the nearest O(2) along the migration path of H1. The red arrows identify the transition state of the proton between the hydrogen atoms $O(2)^1$ and $O(2)^2$.

$(SeO_4)^3$. At the transfer of H1 between $O(2)^2$ and $O(2)^3$, the lengths of the bonds Se-$O(2)^3$ (vertex oxygen) and Se-$O(1)^3$ (basis oxygen) in the group $(SeO)^3$ are also changed by about 0.08–0.16 Å. After the proton is transferred from $O(2)^2$ to $O(2)^3$, the length of the Se-$O(2)^2$ bond is returned to its previous value, 1.76 Å.

Figure 11 demonstrates the redistribution of the valence charge density during the migration of the hydrogen. The intrabond proton transfer step between the vertex oxygens $O(2)^1$ and $O(2)^2$ corresponds to the contours (a)–(d) of the plot. One can see that the hydrogen transfer has a character of a continuous redistribution of the electronic charge density between the two different positions near $O(2)^1$ and near $O(2)^2$ detected in Figs. 11(b) and 11(c). This finding allows us to improve the conclusions of the neutron-scattering studies in Ref. 30 about the absence of the two distinct proton positions within a hydrogen bridge in the conducting phase of $Rb_3H(SeO_4)_2$ that can be explained by the limited resolution of the experiments. Furthermore, in the rotational step [Figs. 11(d)–11(f)], the rotational displacements of the oxygen $O(2)^2$ follow the proton rotation and lead to significant modifications of the charge density contours near $O(2)^2$ that obtain a distinct dumbbell character.

TABLE II. Hydrogen bond parameters [minimal and maximal O(2)-O(2) distances d_{OO}^{min} and d_{OO}^{max} in Å], protonic polaron transport parameter ∇V (eV/Å) and the transport activation energy E_a(eV) in the superionic phase of $Rb_3H(SeO_4)_2$ calculated by the NEB method and estimated experimentally.

Method	d_{OO}^{min}	d_{OO}^{max}	$\nabla V = \frac{\partial E}{\partial \Delta_O}$	E_a
NEB (full relaxation)	2.51	2.7	2.55	0.33
Refs. 17 and 29	2.4	2.7	–	0.37
Ref. 15	2.51	2.67	–	0.49

As a consequence of our findings, we propose that significant displacements of the oxygens O(2) during the migration of the hydrogen are an additional feature of the proton transport mechanism. It is also remarkable that the well-established standard Grotthuss proton transport mechanism contains two main (rotational and translational) stages and does not involve oxygen displacement as a decisive factor in the proton migration process, which contradicts the results of the present work.

To see the role of O(2) displacement in establishing hydrogen transport, we examine more closely the change of the total system energy along the proton migration path presented in Fig. 9. Figure 9 shows that the energy barrier for the hydrogen rotation step approaches 0.2 eV and is substantially lower than the barrier for the proton transfer between neighboring groups that is about 0.6 eV in Fig. 9(b). The relation between the obtained rotation and translation barriers is consistent with the conclusion about the decisive role of the intrabond proton transfer in the determining the activation energy for proton conductivity reported in Refs. 9 and 17.

In $M_3H(XO_4)_2$ systems, the dominant role of the intrabond translational step in the formation of the transport activation energy is in contrast to the quasi-one-dimensional proton conductors $MHXO_4$, where the proton conduction process is determined by the rotational energy barriers. This fact is also supported by the recent DFT studies of $CsHSO_4$[24] where the intrabond proton barrier 0.16 eV was found to be substantially lower than the rotational barrier 0.52 eV and is also consistent with the *ab initio* molecular dynamics calculations of the related systems[35] that show strong fluctuations of the hydrogen bond lengths between 2.4 and 2.8 Å during the proton migration and fast almost barrierless proton transfer on the hydrogen bonds characterized by the extremely short lengths about 2.4 Å. The fast intrabond proton transfer in the quasi-one-dimentional proton conductors is similar to the proton transport properties in water mixtures where the recent *ab initio* molecular dynamics simulations demonstrate the existence of two different time scales and identify the faster process with the intrabond proton transfer, while the slower time scale corresponds to local rearrangements of the hydrogen-bond network.[36] In this context, the unique two-dimensional character of the transport mechanism in the $M_3H(XO_4)_2$ introduces qualitative changes in the translational and rotational energy barriers with a consequent importance of the intrabond transfer in the determination of the transport energy barriers.

The change of the total energy profile along the transfer path in Fig. 9(b) can be directly compared with the corresponding displacements of hydrogen bonded O(2) in Fig. 10(a). From this comparison, we obtain that the increase of the total energy up to $\Delta_E = 0.55$ eV is accompanied by the O(2) displacements $\Delta_O = 0.25$ Å. In the phenomenological description of the proton transport,[21] the antiphase displacements of O(2) induced by the hydrogen-bonded proton have been classified in terms of the "proton-polaronic" effect where the protonic polaron is formed due to the interactions of proton with the antiphase stretching displacements of the nearest O(2) oxygens and the energy for the formation of the protonic polaron $E_0 = (\hbar \nabla V)^2/2M(\omega_0)^2$ depends on the energetic parameter

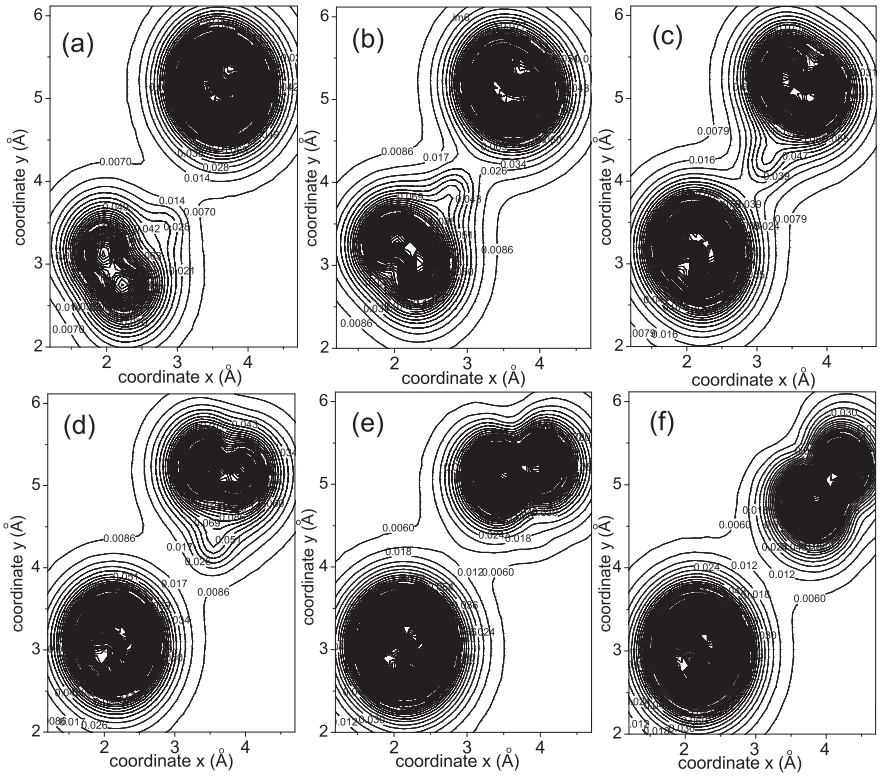

FIG. 11. Electronic density contours showing the redistribution of the valence charge density of the hydrogen bond $O(2)^1$-H-$O(2)^2$ during the intrabond proton transfer (a)–(d) and during the rotational motion of H covalently bonded to $O(2)^2$ (d)–(f). The valence charge has been obtained by the integration of DOS in the energy window ($E_F - 4$ eV; E_F) where E_F is the Fermi level.

$\nabla V = \partial E/\partial \Delta_O$ (here M is the oxygen mass) and on the characteristic frequency ω_0 of of the O(2)-stretching vibration mode. From the *ab initio*- profiles shown in Figs. 9(b) and 10(a), one can derive the value of $\nabla V = 2.55$ eV Å^{-1} that appears to be very close to the value 2.4 eV Å^{-1} used in the phenomenological calculations in Ref. 21. Using the value $\omega_0 \approx 850\,\text{cm}^{-1}$ which is in the range of the characteristic frequencies of the HSeO4 stretching vibrations of $Rb_3H(SeO_4)_2$ reported in Ref. 37, we obtain the estimate for the protonic polaron binding energy: $E_0 = 0.2$ eV. With this value, using a high-temperature estimate $E_a \approx 5E_0/3$ obtained in the weak proton interaction limit from Ref. 21, we find the activation energy for the proton transport $E_a = 0.33$ eV. Table II compares the activation energies for the proton conductivity derived on the basis of the present DFT calculations and reported in different experimental measurements. The obtained value 0.33 eV is very close to the experiment that confirms a central role of the O(2) distortions for the proton migration mechanism.

It is also worth noting that the snapshot in Fig. 8(d) corresponds to the two protons located near the same ionic group $(SeO_4)^3$, a configuration similar to the high-energy Bjerrum (rotational) defect.[38] The energy barrier for the creation of such types of defects is calculated from the obtained energy profile and is about 1.5 eV, which is twice as high as the estimated translation barrier and which supports negligibly small probability for the creation of the Bjerrum defects in this family of proton conductors.

IV. CONCLUSIONS

We have performed density functional studies of the electronic properties and the mechanisms of hydrogen migrations in the system $Rb_3H(SeO_4)_2$ which belongs to the technologically promising class of proton conductors of the $M_3H(XO_4)_2$ crystal family (M = Rb, Cs, NH_4; X = S,Se). The results of the electronic structure calculations show a central role of the lattice dynamics in the process of the proton migration. Our findings verify several experimental conclusions obtained in the previous x-ray and NMR experiments with $Rb_3H(SeO_4)_2$, which allow us to clarify the positioning of the vertex oxygens O(2) during proton migration and to examine the proton positions on the hydrogen bond at the intrabond proton transfer. The principal conclusion obtained in this work is that the free rotational motion of protons without the corresponding complex distortions of SeO_4 groups cannot be considered an independent part of the Grotthuss transport mechanism. In contrast to the almost free proton motion implemented in a wide range of the models of proton transport, in our work we have considered the migration of hydrogen as a cooperative process that involves a relaxation of the atomic positions and of the distances between the different ionic groups XO_4. We have shown that the migration of the hydrogens is connected with significant displacement of the vertex oxygens O(2). These displacements play a decisive role in the formation of the protonic polaron and in the consequent decrease of the activation energy for the proton conductivity, a concept introduced in the previous phenomenological description of proton transport. The present DFT results allow us to obtain first-principles estimates of the hydrogen bond lengths and energetic parameters involved in the existing phenomenological modeling of the proton transport and to prove the validity of the protonic polaron model. Due to their key role in the formation of new hydrogen bonds and in establishing successful intrabond proton transfer, oxygen displacement should be considered an essential feature of the obtained revised mechanism of the hydrogen

transport. The developed approach can be also implemented for the modeling a wide range of the proton conductors that, in our view, substantially increases the degree of scientific and possible technological applications of the obtained results.

ACKNOWLEDGMENTS

This work was supported through the grants of computer time from the Poznan Supercomputing Center and from the Ukrainian Academic Grid.

[1]T. Norby, Nature **410**, 877 (2001).
[2]S. M. Haile, D. A. Boysen, C. R. I. Chisholm, and R. B. Merle, Nature **410**, 877 (2001).
[3]J. Tollefson, Nature **464**, 1262 (2010); **460**, 442 (2009).
[4]J. S. Hummelshoej *et al*., J. Chem. Phys. **131**, 014101 (2009).
[5]B. Merinov and W. Goddard, J. Chem. Phys. **130**, 194707 (2009).
[6]M. E. Björketun, P. G. Sundell, and G. Wahnström, Phys. Rev. B **76**, 054307 (2007).
[7]Q. Zhang, G. Wahnström, M. E. Björketun, S. Gao, and E. Wang, Phys. Rev. Lett. **101**, 215902 (2008).
[8]A. V. Belushkin, C. J. Carlile, and L. A. Shuvalov, Ferroelectrics **167**, 83 (1995).
[9]R. E. Lechner, Ferroelectrics **167**, 83 (1995).
[10]Y. Yamada, Ferroelectrics **170**, 23 (1995).
[11]A. Bohn, R. Melzer, R. Sonntag, R. E. Lechner, G. Schuk, and K. Lange, Solid State Ionics **77**, 111 (1995).
[12]B. V. Merinov, N. B. Bolotina, A. I. Baranov, and L. A. Shuvalov, Kristallografiya(Crystall. Reports) **33**, 1387 (1988).
[13]B. V. Merinov, A. I. Baranov, and L. A. Shuvalov, Kristallografiya(Crystall. Reports) **35**, 355 (1990).
[14]B. V. Merinov, M. Yu. Antipin, A. I. Baranov, A. M. Tregubchenko, L. A. Shuvalov, and Yu. T. Struchko, Kristallografiya(Crystall. Reports) **36**, 872 (1991).
[15]A. I. Baranov, I. P. Makarova, L. A. Muradyan, A. V. Tregubchenko, L. A. Shuvalov, and V. I. Simonov, Kristallografiya(Crystall. Reports) **32**, 400 (1987).
[16]J. Dolinsek, U. Mikas, J. E. Javorsek, G. Lahajnar, R. Blinc, and L. F. Kirpichnikova, Phys. Rev. B **58**, 8445 (1998).
[17]A. Pietraszko, B. Hilczer, and A. Pawlowski, Solid State Ionics **119**, 281 (1999).
[18]N. M. Plakida and W. Salejda, Phys. Status Solidi B **148**, 473 (1988).
[19]T. Ito and H. Kamimura, J. Phys. Soc. Jpn. **67**, 1999 (1998).
[20]I. V. Stasyuk, N. Pavlenko, and B. Hilczer, Phase Trans. **62**, 135 (1997).
[21]N. I. Pavlenko, J. Phys. Condens. Matter **11**, 5099 (1999).
[22]N. I. Pavlenko and I. V. Stasyuk, J. Chem. Phys. **114**, 4607 (2001).
[23]C. R. I. Chisholm, Y. H. Jang, S. M. Haile, and W. A. Goddard III, Phys. Rev. B **72**, 134103 (2005).
[24]X. Ke and I. Tanaka, Phys. Rev. B **69**, 165114 (2004).
[25]P. Blaha *et al*., *WIEN2K*, *An Augmented Plane Wave + Local Orbitals Program for Calculating Crystal Properties* (TU Wien, Austria, 2001).
[26]J. P. Perdew, K. Burke, and M. Ernzerhof, Phys. Rev. Lett. **77**, 3865 (1996).
[27]J. P. Perdew and A. Zunger, Phys. Rev. B **23**, 5048 (1981).
[28]P. Giannozzi *et al*., J. Phys. Condens. Matter **21**, 395502 (2009).
[29]A. Pawlowski, Cz. Pawlaczyk, and B. Hilczer, Solid State Ionics **44**, 17 (1990).
[30]E. Melzer, T. Wessels, and M. Reehuis, Solid State Ionics **92**, 119 (1996).
[31]H. Jonsson, G. Mills, and K. W. Jacobsen, in *Classical and Quantum Dynamics in Condensed Phase Simulations*, edited by B. J. Berne, G. Ciccoti, and D. F. Coker (World Scientific, Singapore, 1998).
[32]A. I. Baranov, L. A. Shuvalov, and N. M. Shchagina, JETP Letters **36**, 459 (1982).
[33]M. Moakafi, R. Khenata, A. Bouhemadou, H. Khachai, B. Amrani, D. Rached, and M. Rerat, Eur. Phys. J. B **64**, 35 (2008).
[34]N. I. Pavlenko, Phys. Rev. B **61**, 4988 (2000).
[35]H.-S. Lee and M. E. Tuckerman, J. Phys. Chem. C **112**, 9917 (2008).
[36]J. A. Morrone, K. E. Haslinger, and M. E. Tuckerman, J. Phys. Chem. B **110**, 3712 (2006).
[37]A. Pawlowski and M. Polomska, Solid State Ionics **176**, 2045 (2005).
[38]I. V. Stasyuk, O. L. Ivankiv, and N. I. Pavlenko, J. Phys. Stud. **1**, 418 (1997).